Biomaterials 192 (2019) 171–178

Contents lists available at ScienceDirect

Biomaterials

journal homepage: www.elsevier.com/locate/biomaterials

NTA-Co^{3+}-His_6 versus NTA-Ni^{2+}-His_6 mediated E-Cadherin surface immobilization enhances cellular traction

Jacopo Di Russo, Jennifer L. Young, Adithya Balakrishnan, Amelie S. Benk, Joachim P. Spatz*

Max Planck Institute for Medical Research, Department of Cellular Biophysics, Jahnstraße 29, D-69120, Heidelberg, Germany
Department of Biophysical Chemistry, Heidelberg University, INF 253, D-69120, Heidelberg, Germany

ARTICLE INFO

Keywords:
Cobalt
Nitrilotriacetic acid
E-Cadherin
Traction-force
Cell adhesion
Surface functionalization

ABSTRACT

Understanding the biological impact of strategies for protein immobilization onto bioactive surfaces is crucial for the design of biomimetic materials. A common strategy used to immobilize or label recombinant proteins is to exploit the Ni^{2+}-mediated interaction of nitrilotriacetic acid (NTA) with the hexahistidine tag (His_6-tag) present on recombinant proteins. While this method ensures a controlled orientation and functionality of the protein, the kinetically labile nature of the bond ensures only its weak immobilization onto the surface. Recently, it has been shown that the oxidation of Co^{2+} to Co^{3+} greatly stabilizes the bond between NTA and the His_6-tagged proteins, making it inert to ligand exchange and resistant to chelators. This approach not only has the potential to improve the quality of biomimetic material functionalization and molecule labeling but could also affect cellular mechanical responses for which the mechanical strength of the protein-surface bond is crucial. Here, we compared gold (Au) nanopatterned polyacrylamide (PAA) hydrogels functionalized with E-cadherin via Co^{3+} with those functionalized via Ni^{2+} for studying adhesion-mediated responses in keratinocytes. We show that keratinocytes develop higher and a broader range of adhesion forces, leading to extended cell spreading and colony organization on Co^{3+} vs. Ni^{2+}. This work uniquely shows that stabilizing the NTA/His_6-tag bond via Co^{3+} for protein immobilization significantly impacts cellular phenotype on biomimetic materials by impacting cell signaling.

1. Introduction

Biofunctionalization strategies for biomimetic and bioactive materials are largely employed in regenerative medicine and tissue engineering [1–3]. Understanding the biological effects of surface protein functionalization methods is crucial for enabling the best material designs for specific applications e.g. materials design for medical devices and implants or synthetic biology [4,5]. Over recent decades, it has become clear that both the nanoscale properties of a material's surface and the material's physical properties play a pivotal role in controlling a wide range of biological functions, from cell adhesion to more complex changes like stem cell differentiation [2,6]. Thus, the fast-growing mechanobiology field of research has a constant need for technology advancements to better control biophysical parameters.

Several techniques for the exact control of nanoscale ligand spacing and bulk mechanical properties of materials have been published [6,7]. However, the impact of protein immobilization strategies to correctly transmit both of these nano and physical cues is rarely taken into consideration. In the case of cellular adhesion and mechanotransduction in particular, the stability of the immobilized state is important, as traction forces can potentially remove proteins from the surface [8]. This leads to a remodeling of the surface nanostructure, ultimately resulting in alterations to cellular function.

A commonly used strategy to immobilize active proteins on a surface with control over the protein's orientation is to exploit the interaction of nitrilotriacetic acid (NTA) with a hexahistidine tag (His6-tag) [9,10], an amino acid motif that is often attached to recombinant proteins. The interaction between NTA and the His6-tag is possible due to the formation of an octahedral coordination environment mediated by bivalent metal ions such as Ni^{2+} or Co^{2+} [11]. The main advantage of the bond is its high specificity to the His6-tag and the preservation of the attaching protein's integrity. On the other hand, the kinetically labile nature of the interaction makes it easily subjectable to disturbance and ligand exchange, thereby resulting in a bond that can be readily broken [12,13]. For stable immobilization of proteins to surfaces, it is desirable to obtain similar specificity with more stable and kinetically inert interactions.

To obtain this, the binding affinity between histidine chains and NTA can be increased by using multiple NTA molecules, or recombinant proteins with longer His chains (e.g. His10-tag) [14–16]. More recently,

* Corresponding author.
E-mail address: spatz@mr.mpg.de (J.P. Spatz).

https://doi.org/10.1016/j.biomaterials.2018.10.042
Received 12 July 2018; Received in revised form 23 October 2018; Accepted 28 October 2018
Available online 03 November 2018

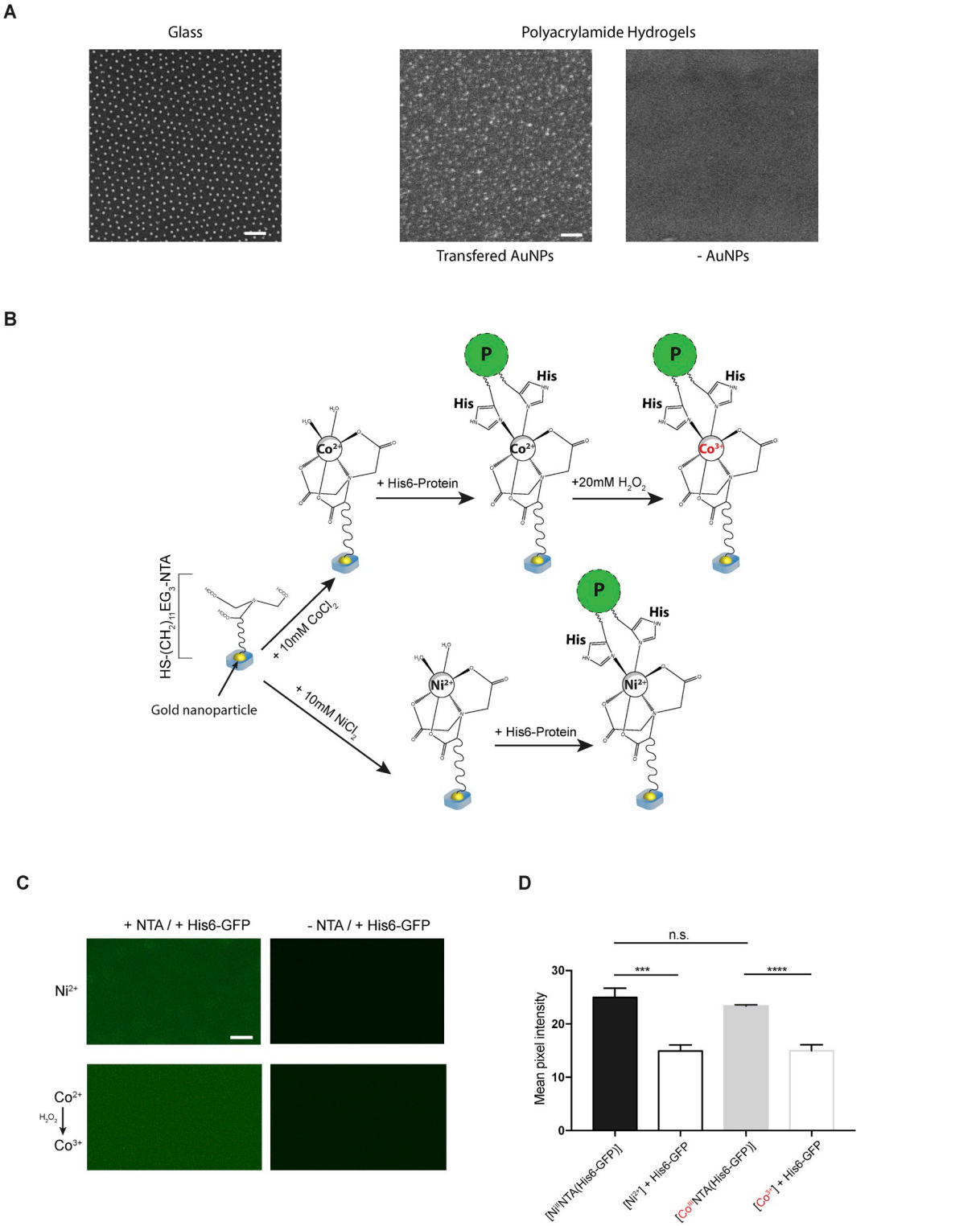

Fig. 1. Characterization of Ni^{2+}- vs. Co^{3+}-mediated protein immobilization strategies on nanopatterned PAA gels. A) Representative scanning electron microscopy images from an Au nanopatterned glass slide (left) and polyacrylamide gels (PAA) after transfer nanolithography (middle) or plain (right). (AuNPs = gold nanoparticles) The scale bar is 100 nm. B) Illustrative scheme showing the experimental steps necessary to immobilize His6-protein on Au nanopatterned gels via HS-(CH_2)11EG3-NTA with $CoCl_2$ and possible oxidation of Co^{2+} to Co^{3+} or $NiCl_2$ (Ni^{2+}) (P = protein). C) Representative fluorescence microscopy images of PAA gels on which His6-GFP was immobilized with Ni^{2+} or Co^{3+} (oxidated from Co^{2+}). No signal was detected on the negative controls without NTA. D) Pixel intensity quantification reveals no significant difference between surface immobilization of His6-GFP via Ni^{2+} ([Ni^{II}NTA(His6-GFP)]) compared to Co^{3+} ([Co^{III}NTA(His6-GFP)]), in contrast to the strong effect of NTA presence vs. absence. Values shown are mean ± s.e.m., resulting from the quantification of at least two fields of view per gel per condition from n = 3 independent experiments. ***p < 0.001, ****p < 0.0001, n. s. = not significant using an unpaired *t*-test. (For interpretation of the references to color in this figure legend, the reader is referred to the Web version of this article.)

a new strategy has been developed where the oxidation of Co^{2+} to Co^{3+} within the coordination environment can considerably improve the stability of the bond between NTA and the His6-tagged protein, rendering it inert to ligand exchange and resistant to chelators [17,18]. In particular, the Co^{3+} allows the NTA-His6-tag bond to reach a dissociation rate constant of 6 order of magnitude lower than with Ni^{2+}, forming a complex with a half-life of 7.1 days [17].

One possible application of this newly developed approach is the immobilization of adhesion proteins such as cadherins. Cadherin cell–cell adhesion proteins mediate homophilic, force-dependent interactions between cells [19]. During the immobilization of cadherins onto artificial surfaces, both the physical properties of the material as well as the mechanical strength of the protein-surface bond are important because cadherins can form catch bonds, whose stability is influenced by tensional forces [20,21].

In this study, we investigated whether the more stable surface

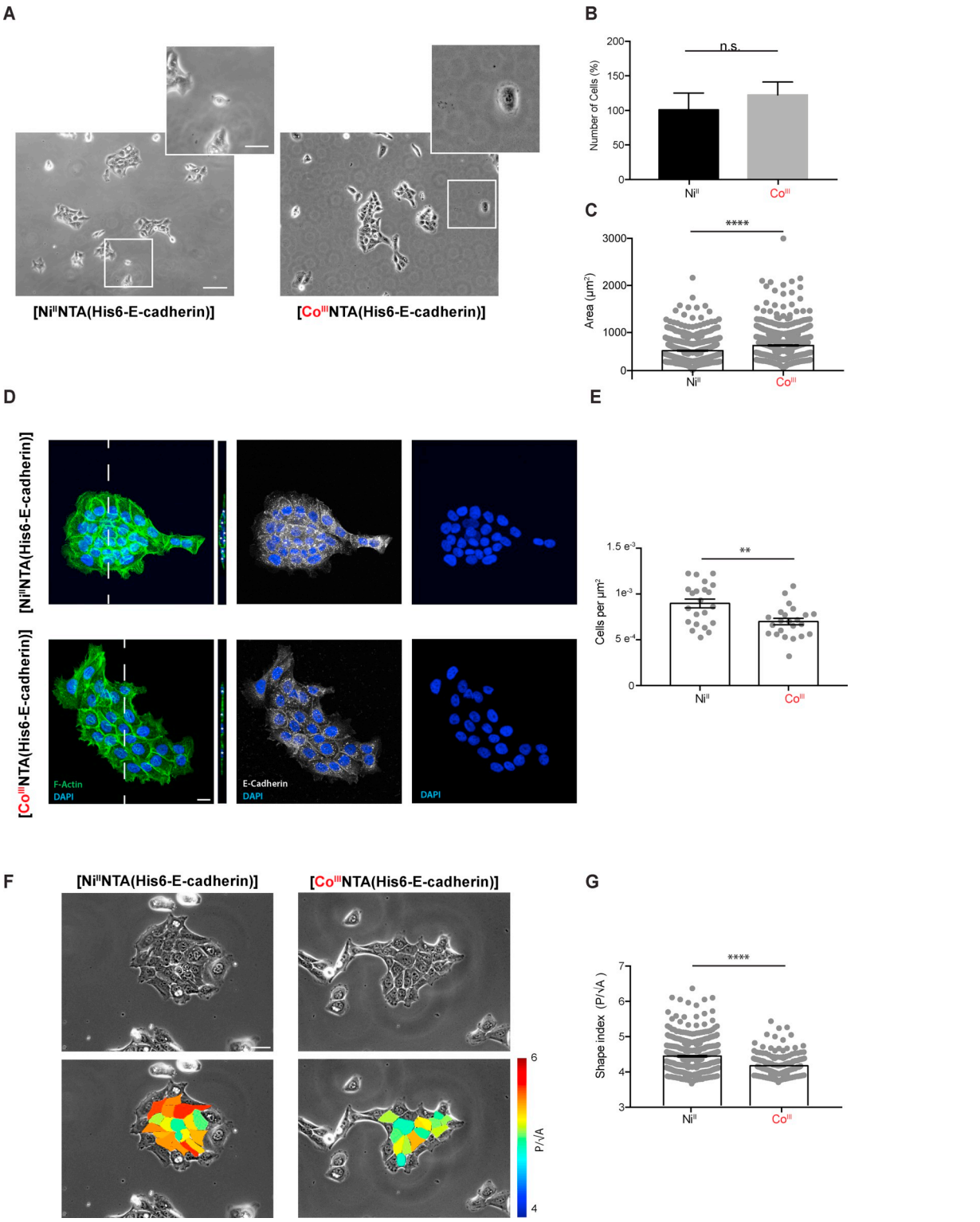

(caption on next page)

Fig. 2. Keratinocyte adhesion on E-cadherin-functionalized PAA gels. A) Representative phase contrast images of Au nanopatterned gel surfaces featuring His6-E-cadherin immobilized via Ni^{2+} or Co^{3+} 24 h after seeding keratinocytes. Boxed areas are shown at higher magnification in the upper right corner of the images. Scale bars are 100 μm and 20 μm in the lower and the upper magnified images, respectively. B) The quantification of number of cells adhering on both surfaces show no significant differences. Values are expressed in mean percentage ± s.e.m of average number of cells adhering on His6-E-cadherin immobilized via Ni^{2+}. The quantification was performed in n = 4 independent experiments. C) The quantification of the cell spread area shows a significantly higher spreading ability of keratinocytes on [Co^{III}NTA(His6-E-cadherin)] compared to [Ni^{II}NTA(His6-E-cadherin)]. Values shown are mean ± s. e.m. for at least 700 cells from n = 3 experiments. ****p < 0.0001 using an unpaired *t*-test with Welch's correction. D) Maximum intensity projection of fluorescently labeled actin cytoskeleton (green), E-Cadherin (white) and blue-labeled nuclei (DAPI) of a representative keratinocyte colony. The images reveal the presence of partial overlap of cells within the colonies formed on [Ni^{II}NTA(His6-E-cadherin)] as better visible by the orthogonal views of the confocal z-stacks. * indicates cellular nuclei. The scale bar is 15 μm. E) The quantification of number of cells per colony area (μm^2) shows a significantly higher cellular density in colonies formed on [Ni^{II}NTA(His6-E-cadherin)]. Values shown are mean ± s.e.m. for at least 20 colonies from n = 4 experiments. **p < 0.01 using an unpaired *t*-test with Welch's correction. F) Representative phase contrast images of keratinocyte colonies on PAA surfaces differing in the His6-E-cadherin immobilization strategy (top), and the same cells color-coded to indicate their shape index (below). The scale bar is 50 μm. The color bar on the right reflects the range of shape indices P/√A from 4 (blue) to 6 (red). G) Quantification of shape indices from cells that make up the interior part of a colony, i.e., cells that are completely surrounded by other cells. Cells on [Co^{III}NTA(His6-E-cadherin)] showed a significantly different and lower shape index compared to cells attached to [Ni^{II}NTA(His6-E-cadherin)]. Values shown are mean ± s.e.m. of at least 450 cells from n = 3 experiments. ****p < 0.0001 using a Mann-Whitney test due to the lack of normal distribution in the data. (For interpretation of the references to color in this figure legend, the reader is referred to the Web version of this article.)

protein immobilization strategy via Co^{3+} has a significant impact on cellular adhesion and traction in comparison to the more common Ni^{2+}-mediated immobilization. In particular, we examined the effect of one of the best-studied members of the cadherin family, epithelial cadherin (E-cadherin), in mediating keratinocyte adhesion and intercellular organization using Au-nanopatterned polyacrylamide (PAA) soft gels.

2. Methods

Fabrication of Au-nanopatterned Glass Surfaces. To create Au-nanopatterned glass coverslips with 35 nm inter-particle spacing, 18 mm diameter glass coverslips (Carl Roth, Germany) were first cleaned in piranha solution (3 H_2SO_4:1 H_2O_2) for 60 min, then rinsed thoroughly in MiliQ water and stored in MilliQ water until further use. A gold micellar solution was prepared as previously described [22] by dissolving diblock copolymer polystyrene (288)-b-poly (2-vinylpyridine) (119) (Polymer Source) in o–xylene at a concentration of 5 mg/mL and subsequent loading with $HAuCl_4 \cdot 3H_2O$ (Sigma Aldrich) at L = 0.5 according to L = n [$HAuCl_4$]/n [P2VP]. The glass coverslips were then spin-coated with 18 μL of the prepared micellar solution at 8000 rpm (WS-650HZ-23NPP/A2/AR2, Laurell Technologies Cooperation) and treated with argon-hydrogen plasma (90% Ar/10% H_2) in a Tepla PS210 microwave plasma system (PVA Tepla, Germany) for 45 min at 200 W and 0.4 mbar in order to remove the polymer.

AuNP Transfer onto Polyacrylamide Hydrogels. Surface nanopatterning of polyacrylamide hydrogels was performed as previously described [22,23]. Briefly, AuNPs on the glass coverslips were first coated with 0.5 mg/ml N, N´-bis(acryloyl)cystamine (Thermo Fisher) in ethanol for 1 h at room temperature in the dark, then washed thoroughly in ethanol and dried with nitrogen. Polyacrylamide (PAA) hydrogel substrates of 23 kPa stiffness were produced by pouring a mixture of 7.5% acrylamide (Bio-Rad), 0.2% bisacrylamide (Bio-Rad), 0.003% Tetramethylethylenediamine (TEMED, Bio-Rad), and 0.03% Ammonium persulfate (Sigma) diluted in PBS onto glutaraldehyde-activated glass bottom dishes (MatTek) and then covering the hydrogel surface with AuNP-functionalized coverslips. To produce PAA hydrogels of 4 kPa stiffness, 5% acrylamide and 0.1% bisacrylamide were used, while all other parameters as mentioned for 23 kPa remained the same. After polymerization, gels were allowed to swell for 72 h in phosphate-buffered saline (PBS) in order to achieve efficient particle transfer and facilitate the separation of the coverslip from the gel. Transfer efficiency was evaluated by scanning electron microscopy (SEM) of both the glass surface and the gels.

Characterization of Au-nanopatterned Surfaces. All nanopatterned substrates were evaluated by SEM, as previously described [22,23], in order to determine inter-particle spacing and particle order. Hydrogels and the removed coverslips were also evaluated for particle transfer efficiency. Hydrogels were prepared for SEM evaluation using a CPD 030 critical point dryer (CPD, BAL-TEC). Briefly, the hydrogels were dehydrated by gentle agitation in solutions containing increasing concentrations of EtOH/H_2O (10% v/v, 30%, 50%, 70%, 90%, 95%), followed by three washing steps in 100% EtOH. Then the samples were promptly transferred to a CPD chamber, EtOH was exchanged with liquid CO_2, and samples were dried above the critical point. All samples – i.e., AuNP coverslips that had not been used for particle transfer, AuNP CPD-dried hydrogels and the coverslips after particle transfer to hydrogels – were sputter-coated with carbon (Low Vacuum Coater EM ACE200, Leica) and inspected in an Ultra 55 F E-SEM featuring a Gemini column (Carl Zeiss) using an in-lens detector at accelerating voltages of 3–5 kV and a working distance of ~6 mm. Images were quantified for both inter-particle spacing and overall bond orientation order employing the K-Nearest-Neighbors algorithm. To this end, the k-nearest neighbors (k = 6 for ordered particles) were calculated using an in-house script written in ImageJ (National Institutes of Health) for > 600 particles per sample. The glass coverslips that had been used to produce nanostructured hydrogels were inspected to confirm the efficient transfer of the AuNPs onto the hydrogel surface, i.e., they retained little to no AuNP residues.

Functionalization of Patterned Hydrogels. Gels were sterilized under UV for 30 min before being incubated in 1 mM thiolated nitrilotriacetic acid (HS-$(CH_2)_{11}$-EG_3-NTA, Prochimia Surfaces, cat. TH007) for 1 h at room temperature. The gels were washed once with ddH_2O and twice with Hank's Balanced Salt Solution (HBSS) before being incubated with the metal solutions for 30 min at room temperature. In the case of Ni^{2+}-mediated complexes, the gels were incubated in 10 mM $NiCl_2$ (Merck) diluted in HBSS. For $Co^{2+/3+}$-mediated complexes, the gels were incubated in 10 mM $CoCl_2 \cdot 6H_2O$ (Sigma Aldrich) diluted in degassed HBSS. The gels were washed in HBSS and incubated for 1 h at room temperature with either 10 μg/mL of His6-Green Fluorescent Protein (Thermo Fisher, cat. 13,105-S07E) for direct fluorescence imaging or 10 μg/ml of recombinant human His6-E-cadherin (extracellular domain (Asp155-Ile707) with a C-terminal His6-tag, UniProtKB P12830; R&D systems, cat. 8505-EC-050) for cell studies. In order to oxidate Co^{2+} to Co^{3+} and for the control experiments, the gels were incubated for 1 h with 20 mM H_2O_2, then thoroughly washed with HBSS. For NHDF adhesion studies sterilized gels were incubated with 25 μM custom-synthesized cRGD-thiol peptide, (cyclo [Arg–Gly–Asp]–D–Phe–Lys-$[PEG]_{18}$-$[Cys]_3$, Peptide Specialty Laboratories, PSL) at room temperature for 2 h, washed with PBS and then used for cell seeding.

Cell Culture. Human immortalized keratinocytes (HaCat, Cell Line Service) were cultured in Dulbecco's Modified Eagle Medium (DMEM, Gibco) supplemented with 10% Fetal Bovine Serum (FBS, Sigma Aldrich) and 1% Penicillin-Streptomycin (P/S, Gibco) at 5% CO_2 and 37 °C. Primary Normal Human Dermal Fibroblasts from an adult donor

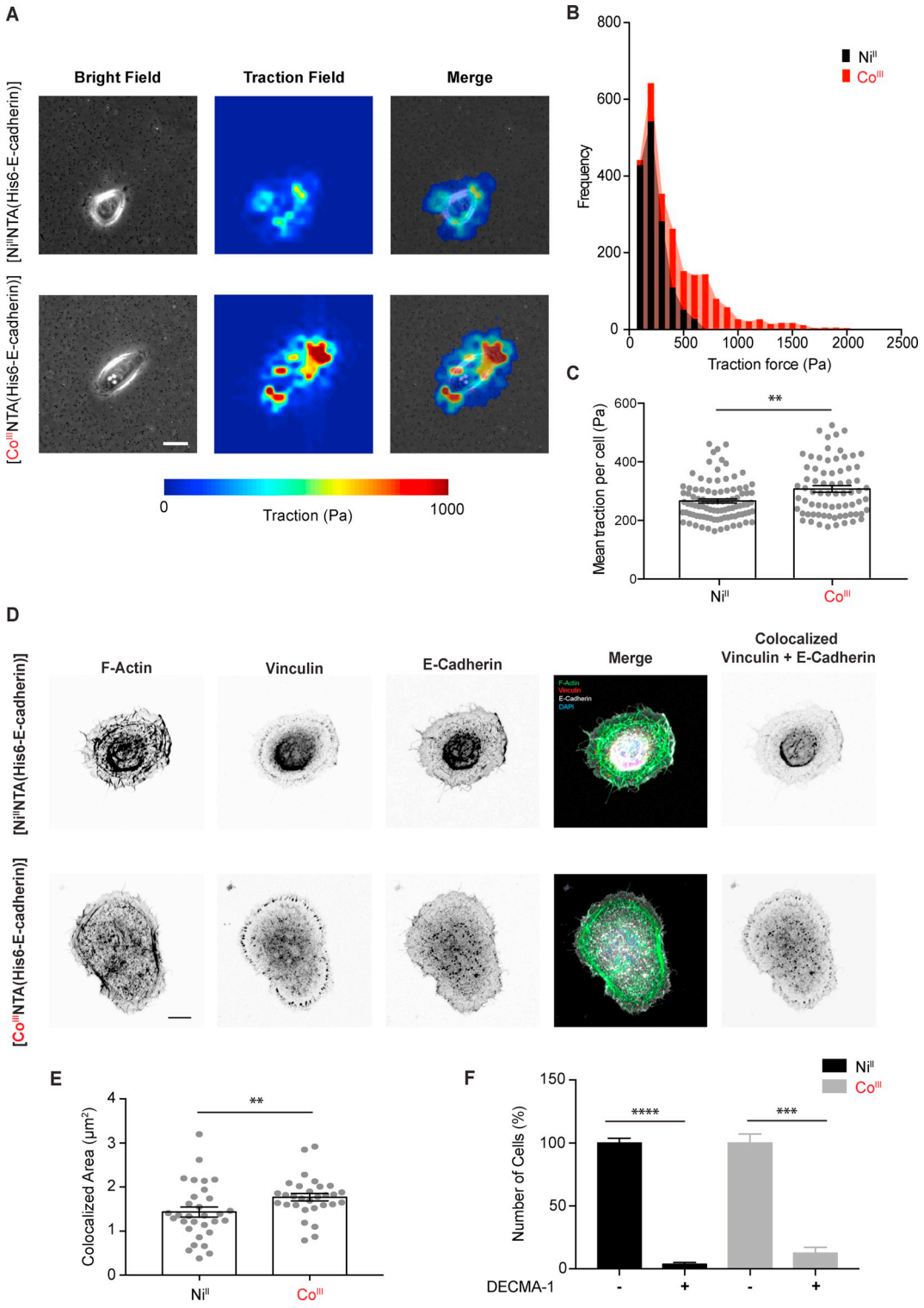

Fig. 3. Keratinocyte E-cadherin adhesion forces are higher on [Co^{III}NTA(His6-E-cadherin)]. A) Representative phase contrast images of single keratinocytes on PAA gels functionalized with His6-E-cadherin via Ni^{2+} or Co^{3+}, and the corresponding traction force profiles. The scale bar is 20 μm. B) Frequency distribution of the traction forces quantified in A shows a broader and higher range of tractions developed on [Co^{III}NTA(His6-E-cadherin)]. C) Quantification of average traction force (Pa) developed by each cell shows significantly higher forces on [Co^{III}NTA(His6-E-cadherin)]. Values shown are mean ± s. e.m. of at least 70 cells from n = 3 experiments. **p < 0.01 using a Mann-Whitney test due to the lack of normal distribution in the data. D) Representative fluorescence images of keratinocytes seeded on PAA surfaces functionalized with His6-E-cadherin via Ni^{2+} or Co^{3+}, stained for F-actin (green in colorized image), Vinculin (red in colorized image), E-cadherin (white in colorized image) and DAPI (blue in colorized image). The images in the far right-hand column represent the colocalized pixels between Vinculin and E-cadherin. The scale bar is 10 μm. E) Quantification of Vinculin/E-Cadherin structures based on the colocalized pixels present at the cells boundaries. Cells adhering to [Co^{III}NTA(His6-E-cadherin)] show significantly bigger structures compared to cells adhering to [Ni^{II}NTA(His6-E-cadherin)]. Values shown are mean ± s.e.m. sizes per cell from at least 30 cells and n = 3 experiments. **p < 0.01 using a Mann-Whitney test due to the lack of normal distribution in the data. F) Adhesion assay performed on keratinocytes in the presence of E-Cadherin blocking antibody. The values are expressed as percentage mean ± s.e.m. of the corresponding controls from n = 3 independent experiments. ***p < 0.001, ****p < 0.0001 using an paired *t*-test with Welch's correction. (For interpretation of the references to color in this figure legend, the reader is referred to the Web version of this article.)

(NHDF, Promocell, cat. C-12302) were cultured in fibroblast growth medium (Promocell, cat. C-23020) at 5% CO_2 and 37 °C. For experiments, cells were detached, re-suspended to obtain a seeding density of 60,000 cells/cm^2, and allowed to spread overnight on the functionalized gels before further analyses.

Traction Force Microscopy (TFM). TFM was performed as described previously [24]. Briefly, a suspension of 0.5 μm fluorescent carboxylated polystyrene beads (Sigma) was added to the casting solution for Au-nanopatterned PAA gels. Fluorescent bead displacement vectors were obtained by subtracting the picture of relaxed beads (cell-free gel after trypsinization) from the picture acquired with cells. Traction forces were calculated from these vectors using an ImageJ plugins (PIV, FTCC) and MATLAB was used to graphically represent the traction force fields [24].

Immunofluorescence Microscopy. Cells on gels were fixed with ice-cold 4% paraformaldehyde in PBS for 10 min at 4 °C, permeabilized with 0.2% Triton X-100 for 2 min at room temperature and blocked for 30 min with 1% bovine serum albumin (BSA) in PBS. Cells were then incubated with primary antibodies or Alexa Fluor™ 488 Phalloidin (Thermo-Fisher, cat. A12379, 1:200) diluted in PBS containing 1% BSA overnight at 4 °C, washed in PBS and subsequently incubated for 2 h at room temperature with secondary antibodies diluted in PBS containing 1 μg/ml DAPI (Thermo-Fisher, 62,248). The following primary antibodies and concentrations were employed: rabbit anti-human vinculin (Abcam, cat. ab73412, 5 μg/ml) and mouse anti-human E-Cadherin (BD transduction laboratories, cat. 610,182, 5 μg/ml). The following secondary antibodies were employed: Alexa Fluor™ 647 goat anti-mouse IgG (Thermo-Fisher, A21235, 4 μg/ml) and Alexa Fluor™ 594 goat anti-rabbit IgG (Thermo-Fisher, A11012, 4 μg/ml). Images were acquired using a Leica SP5 confocal laser-scanning microscope and maximum intensity projections were obtained with Imaris software (Bitplane, Oxford Instruments).

Adhesion Assay. Cells were trypsinized and resuspended at a concentration of 10^6 cells per ml in ice-cold culture medium containing 20 μg/ml of E-Cadherin blocking antibody (DECMA-1, Millipore, MABT26). After 15 min incubation on ice, the cells were seeded on the surfaces in medium containing 10 μg/ml of E-Cadherin blocking antibody and allowed to attach for 30min (for [Co^{III}NTA(His6-E-cadherin]) or 1.5 h (for [Ni^{II}NTA(His6-E-cadherin]) before gently washing with PBS containing calcium and magnesium. The remaining cells were fixed with 4% paraformaldehyde in PBS for 10 min at 4 °C and stained with DAPI for quantification. Control cells were similarly treated with the exception of the addition of the E-Cadherin antibody in the medium.

Image analyses. Phase contrast and fluorescence cell images were acquired with an Axiovert 200 M or an Imager. Z1 (Carl Zeiss AG, Germany) and analysed for adhesion area and perimeter using ImageJ software or for cell numbers and size of Vinculin/E-Cadherin structures using Imaris (Bitplane) software.

Statistic. Statistic tests were performed using the software Prism (GraphPad). Parametric or not-parametric tests were chosen after evaluating the normality distribution of the data.

3. Results and discussion

To mimic the stiffness of tissues and the cellular physiological environment, experiments were performed on 23 kPa polyacrylamide (PAA) hydrogels. These were nanopatterned with Au nanoparticles (AuNPs) of ~6 nm diameter, which were uniformly distributed onto the surface with an inter-ligand spacing of ~36 nm (36 ± 6.4 nm). This distance was chosen because it is biologically relevant for cell adhesion [23,25] and it creates a dense surface functionalization. First, Au nanopatterns were fabricated on glass slides via block copolymer micelle nanolithography (BCMN) [26] (Fig. 1A, left panel) and then transferred onto PAA gels (Fig. 1A, middle panel) using N, N′-bis(acryloyl)cystamine. This process leads to Au nanoparticle incorporation into the gel surface during polymerization [22]. Successful transfer was evaluated by scanning electron microscopy (SEM) of the hydrogels after transfer in comparison with plain hydrogels (Fig. 1A middle and right panels).

Protein immobilization was optimized on Au-nanopatterned PAA gels using green fluorescent protein with a N-terminal his-tag (His6-GFP), as illustrated in the experimental scheme in Fig. 1B. AuNPs were functionalized with NTA-SH, modified through the addition of metal salts (either $NiCl_2$ or $CoCl_2$), and coupled to the His6-protein. Both $NiCl_2$ and $CoCl_2$ (before and after oxidation) are similarly efficient in terms of the amount of NTA-mediated protein immobilized on the surface [17,18]. However, to ensure this also holds true for AuNPs on PAA gels, we examined the surfaces using fluorescence microscopy after His6-GFP immobilization (Fig. 1C). Quantification of the fluorescence intensity did not show any significant differences between Ni^{2+} and Co^{3+}-mediated immobilization (Fig. 1D), suggesting comparable protein densities.

The immobilization of His6-tagged proteins via surface-bound NTA is advantageous for biological studies because the location of the His6-tag in the protein can be genetically manipulated, thereby allowing for control over protein orientation upon surface binding via NTA. Cadherins represent one group of cell adhesion proteins whose orientation is crucial for their function [20,27]. The best-studied member of this group is epithelial cadherin (E-cadherin), which is crucial for epithelial integrity and function [27] and thus widely used in the development of biomimetic materials [28,29]. Hence, we decided to test whether Co^{3+}-mediated protein immobilization would have a significant impact on E-cadherin-mediated cell adhesion compared to the classically used Ni^{2+}-dependent strategy.

To study this, we immobilized the recombinant human extracellular fragment of E-cadherin via its C-terminal His6-tag, thereby allowing the homophilic binding domains at the N-terminus to be free for interaction with cellular E-cadherins. Human keratinocytes (HaCaT) were seeded onto PAA gels that were functionalized with E-cadherin by either Ni^{2+} or Co^{3+} as the binding mediator. Keratinocytes successfully bound on both surfaces in a comparable manner (Fig. 2A and B), thereby confirming the functionality of both protein immobilization strategies. We did, however, observe differences in cell morphology for both single cells and cell colonies (Fig. 2). On substrates functionalized with E-cadherin using trivalent Co^{3+} ([Co^{III}NTA(His6-E-cadherin]), single cells exhibit a significantly higher adhesion area compared to cells on substrates where E-cadherin was immobilized using bivalent ions, namely Ni^{2+} ([Ni^{II}NTA(His6-E-cadherin)]) or Co^{2+} ([Co^{II}NTA(His6-E-cadherin)]) (Fig. 2A and C; Supplementary Fig. 1A). In addition, cell colonies appeared to be better organized in honeycomb-like structures on [Co^{III}NTA(His6-E-cadherin)] compared to [Ni^{II}NTA(His6-E-cadherin)] when observed by light microscopy and fluorescence microscopy after staining for F-actin and E-cadherin to be able to better identify cell boundaries (Fig. 2D and F).

To quantify this observation, we first counted the number of cells per colony extension area, showing a significantly higher cell density in cell colonies on [Ni^{II}NTA(His6-E-cadherin)] compared to [Co^{III}NTA(His6-E-cadherin)], which is due to cellular overlapping on [Ni^{II}NTA(His6-E-cadherin)] (Fig. 2D and E). Furthermore, we used a non-dimensional shape index q, which is calculated by taking the ratio of the cell perimeter P to the square root of its area A ($q = P/\sqrt{A}$) [30]. This shape index has been shown to describe intercellular stresses in relation to cell-extracellular matrix tractions. Lower shape index is the result of higher intercellular stresses within an epithelial monolayer or, in this case, of a cell colony. In epithelia, this lower shape index correlates to a jammed honeycomb cellular configuration [30]. The shape index of those cells located within the colonies (Fig. 2F) was significantly lower on substrates functionalized with E-cadherin using the trivalent Co^{3+} [Co^{III}NTA(His6-E-cadherin)] compared to those functionalized using bivalent Ni^{2+} [Ni^{II}NTA(His6-E-cadherin)] or Co^{2+} [(Co^{II}NTA(His6-E-cadherin)] (Fig. 2F and G; Supplementary Fig. 1B).

The observed differences in cell adhesion area and colony

organization suggest that the strength of cellular adhesion is altered by the stability of the metal ion used to immobilize E-cadherin. In addition, intercellular stresses have been positively correlated with cell-surface traction forces [31,32]. Thus, we sought to determine if the morphological differences of keratinocytes on [Co^{III}NTA(His6-E-cadherin)] surfaces were the result of a stronger adhesion to the functionalized gel caused by increased protein stability on the surface. To quantify cellular adhesion strength, we performed traction force microscopy (TFM) by incorporating fluorescent beads in the nanopatterned PAA gels (Fig. 3A–C) and measured the forces developed by single keratinocytes. We found that cells seeded on [Co^{III}NTA(His6-E-cadherin)] developed higher traction forces than cells seeded on [Ni^{II}NTA(His6-E-cadherin)] or [Co^{II}NTA(His6-E-cadherin)] (Fig. 3A–C; Supplementary Fig. 1C). These differences in traction forces were also present on softer PAA gels (4 kPa) indicating that the effect is independent of the substrate's properties (Supplementary Fig. 1E). The data suggest that stabilizing the bond between E-cadherin and the gel surface alone is sufficient to set a higher force threshold for cellular adhesion as confirmed by the more frequent higher traction forces measured in the cell on [Co^{III}NTA(His6-E-cadherin)] (Fig. 3B). This higher force threshold is conferred by the type of metal ion used to connect NTA and the His6-tag, in this case more stable Co^{3+} in contrast to less stable Ni^{2+} or Co^{2+}.

We further investigated the nature of surface cell adhesion by immunofluorescence staining of focal adherens junction components in the adhered keratinocytes (Fig. 3D). These mechanoresponsive structures are normally present during the formation, remodeling and disruption of cell-cell adhesion, and are characterized by actin fibers connected to E-cadherin via adaptive proteins such as vinculin [33]. On [Ni^{II}NTA(His6-E-cadherin)] and [Co^{III}NTA(His6-E-cadherin)], the data show a spatial correlation between both vinculin and E-cadherin complexes with actin fibers, suggesting that focal adherens junctions mediate cell adhesion on these substrates. The quantification of the junctions' size showed that Vinculin/E-Cadherin structures were significantly larger on [Co^{III}NTA(His6-E-cadherin)] vs. [Ni^{II}NTA(His6-E-cadherin)] (Fig. 3E), thus confirming higher adhesion of cells on the [Co^{III}NTA(His6-E-cadherin)] surface compared to the [Ni^{II}NTA(His6-E-cadherin)] surface.

In order to ensure that the increased traction force measured on [Co^{III}NTA(His6-E-cadherin)] was a direct result of the new immobilization method rather than a secondary effect of the surface chemistry, we tested whether the mild oxidation step necessary to immobilize His6-E-cadherin via Co^{3+} resulted in a higher affinity of E-cadherin homodimer formation regardless of the metal ion mediator. Oxidizing Ni^{2+} to Ni^{3+} does not improve the stability of the NTA-His6-tag interaction due to the different chemical properties of Nickel; therefore, we compared cells seeded on [Ni^{II}NTA(His6-E-cadherin)] functionalized hydrogels with or without 20 mM H_2O_2 treatment. Quantification of traction forces showed no significant difference between the two conditions, confirming that the mild oxidation step does not affect E-cadherin adhesion properties (Supplementary Fig. 1D).

Finally, we tested the specificity of the surface functionalization first performing an adhesion assay using the E-Cadherin blocking antibody DECMA-1 [34] and secondly using human primary dermal fibroblasts (NHDF), which express only N-Cadherin, and has been shown to be able to interact with E-Cadherin. Keratinocytes adhesion was blocked by the presence of DECMA-1 in the medium, indicating the specificity of the adhesion (Fig. 3F). NHDF adhesiveness on E-cadherin functionalized surfaces was compared with Au-nanopatterned PAA gels functionalized with thiolated cyclic RGD peptide (cRGD-SH) (Supplementary Fig. 2A and B). As expected, the fibroblasts are highly adhesive to the cRGD-functionalized surface but do not interact efficiently with E-cadherin-functionalized surfaces (Supplementary Fig. 2A and B). Thus, the data confirm the high specificity of both [Ni^{II}NTA(His6-E-cadherin)] and [$Co^{II/III}$NTA(His6-E-cadherin)] binding.

4. Conclusion and remarks

Our data show the biological relevance of using a stable protein immobilization strategy on biomimetic material surfaces. In particular, we show that using trivalent Co^{3+} to mediate NTA binding of E-cadherin (rather than bivalent Ni^{2+} or Co^{2+}) significantly impacts the mechanical response and organization of the cell. Keratinocytes not only attach better on the surface (Fig. 2A and C) but also organize more readily into colonies that reassemble a healthy cubical epithelium (Fig. 3D and F) [30]. This is due to fact that cells can develop higher and a broader range of traction forces on the surface functionalized with [Co^{III}NTA(His6-E-cadherin)] independently by its stiffness (Fig. 3A–C; supplementary fig. 1E). We speculate that the higher bond stability of [Co^{III}NTA(His6-E-cadherin)] is responsible for this observed difference in the keratinocytes' mechanical response. The results found here further underline the potential of employing Co^{3+} for surface functionalization when dealing with proteins that require subjugation to mechanical stresses for proper function, e.g., cell-cell adhesion proteins. Co^{3+}-mediated protein immobilization allows cells to develop a broader range of traction forces, influencing cellular function and better mimicking physiological situations. This is especially important when developing a strategy for surface functionalization that aims to transmit both biochemical and biophysical information to the biological system.

Acknowledgments

The Max Planck Society is appreciated for its general support in all aspects of our research. J.P.S. is the Weston Visiting Professor at the Weizmann Institute of Science and part of the excellence cluster CellNetworks at the University of Heidelberg. We thank Dr. Philippe Girard for the discussion on E-cadherin immobilization, Johannes Hirte and Ioanis Grigoridis for BCMN and SEM technical support.

Appendix A. Supplementary data

Supplementary data to this article can be found online at https://doi.org/10.1016/j.biomaterials.2018.10.042.

References

[1] Z.W. Ma, Z.W. Mao, C.Y. Gao, Surface modification and property analysis of biomedical polymers used for tissue engineering, Colloids Surf., B 60 (2) (2007) 137–157.
[2] S. Cosson, E.A. Otte, H. Hezaveh, J.J. Cooper-White, Concise review: tailoring bioengineered scaffolds for stem cell applications in tissue engineering and regenerative medicine, Stem Cells Transl Med 4 (2) (2015) 156–164.
[3] S.R. Meyers, M.W. Grinstaff, Biocompatible and bioactive surface modifications for prolonged in vivo efficacy, Chem. Rev. 112 (3) (2012) 1615–1632.
[4] K. Göpfrich, I. Platzman, J.P. Spatz, Mastering complexity: towards bottom-up construction of multifunctional eukaryotic synthetic cells, Trends Biotechnol. 36 (9) (2018) 938–951.
[5] G. Wu, P. Li, H. Feng, X. Zhang, P.K. Chu, Engineering and functionalization of biomaterials via surface modification, J. Mater. Chem. B 3 (10) (2015) 2024–2042.
[6] X. Guan, M. Avci-Adali, E. Alarcin, H. Cheng, S.S. Kashaf, Y. Li, A. Chawla, H.L. Jang, A. Khademhosseini, Development of hydrogels for regenerative engineering, Biotechnol. J. 12 (5) (2017).
[7] M. Singh, C. Berkland, M.S. Detamore, Strategies and applications for incorporating physical and chemical signal gradients in tissue engineering, Tissue Eng. B Rev. 14 (4) (2008) 341–366.
[8] Z. Avnur, B. Geiger, The removal of extracellular fibronectin from areas of cell-substrate contact, Cell 25 (1) (1981) 121–132.
[9] M.H. Seo, J. Han, Z. Jin, D.W. Lee, H.S. Park, H.S. Kim, Controlled and oriented immobilization of protein by site-specific incorporation of unnatural amino acid, Anal. Chem. 83 (8) (2011) 2841–2845.
[10] F. Rusmini, Z. Zhong, J. Feijen, Protein immobilization strategies for protein biochips, Biomacromolecules 8 (6) (2007) 1775–1789.
[11] H. Block, B. Maertens, A. Spriestersbach, N. Brinker, J. Kubicek, R. Fabis, J. Labahn, F. Schafer, Immobilized-metal affinity chromatography (IMAC): a review, Methods Enzymol. 463 (2009) 439–473.
[12] T.T. Le, C.P. Wilde, N. Grossman, A.E. Cass, A simple method for controlled immobilization of proteins on modified SAMs, Phys. Chem. Chem. Phys. 13 (12) (2011) 5271–5278.
[13] J. Porath, J. Carlsson, I. Olsson, G. Belfrage, Metal chelate affinity chromatography,

a new approach to protein fractionation, Nature 258 (5536) (1975) 598–599.
[14] S. Lata, M. Gavutis, R. Tampe, J. Piehler, Specific and stable fluorescence labeling of histidine-tagged proteins for dissecting multi-protein complex formation, J. Am. Chem. Soc. 128 (7) (2006) 2365–2372.
[15] A.N. Kapanidis, Y.W. Ebright, R.H. Ebright, Site-specific incorporation of fluorescent probes into protein: hexahistidine-tag-mediated fluorescent labeling with (Ni (2+):nitrilotriacetic Acid (n)-fluorochrome conjugates, J. Am. Chem. Soc. 123 (48) (2001) 12123–12125.
[16] S. Lata, A. Reichel, R. Brock, R. Tampe, J. Piehler, High-affinity adaptors for switchable recognition of histidine-tagged proteins, J. Am. Chem. Soc. 127 (29) (2005) 10205–10215.
[17] S.V. Wegner, J.P. Spatz, Cobalt(III) as a stable and inert mediator ion between NTA and His6-tagged proteins, Angew Chem. Int. Ed. Engl. 52 (29) (2013) 7593–7596.
[18] S.V. Wegner, F.C. Schenk, J.P. Spatz, Cobalt(III)-Mediated permanent and stable immobilization of histidine-tagged proteins on NTA-functionalized surfaces, Chemistry 22 (9) (2016) 3156–3162.
[19] C. Yoshida, M. Takeichi, Teratocarcinoma cell adhesion: identification of a cell-surface protein involved in calcium-dependent cell aggregation, Cell 28 (2) (1982) 217–224.
[20] S. Rakshit, Y. Zhang, K. Manibog, O. Shafraz, S. Sivasankar, Ideal, catch, and slip bonds in cadherin adhesion, Proc. Natl. Acad. Sci. U. S. A. 109 (46) (2012) 18815–18820.
[21] A.V. Priest, O. Shafraz, S. Sivasankar, Biophysical basis of cadherin mediated cell-cell adhesion, Exp. Cell Res. 358 (1) (2017) 10–13.
[22] S.V. Graeter, J. Huang, N. Perschmann, M. Lopez-Garcia, H. Kessler, J. Ding, J.P. Spatz, Mimicking cellular environments by nanostructured soft interfaces, Nano Lett. 7 (5) (2007) 1413–1418.
[23] R. Oria, T. Wiegand, J. Escribano, A. Elosegui-Artola, J.J. Uriarte, C. Moreno-Pulido, I. Platzman, P. Delcanale, L. Albertazzi, D. Navajas, X. Trepat, J.M. Garcia-Aznar, E.A. Cavalcanti-Adam, P. Roca-Cusachs, Force loading explains spatial sensing of ligands by cells, Nature 552 (7684) (2017) 219–224.
[24] T. Das, K. Safferling, S. Rausch, N. Grabe, H. Boehm, J.P. Spatz, A molecular mechanotransduction pathway regulates collective migration of epithelial cells, Nat. Cell Biol. 17 (3) (2015) 276–287.
[25] E.A. Cavalcanti-Adam, T. Volberg, A. Micoulet, H. Kessler, B. Geiger, J.P. Spatz, Cell spreading and focal adhesion dynamics are regulated by spacing of integrin ligands, Biophys. J. 92 (8) (2007) 2964–2974.
[26] R. Glass, M. Moller, J.P. Spatz, Block copolymer micelle nanolithography, Nanotechnology 14 (10) (2003) 1153–1160.
[27] T. Lecuit, A.S. Yap, E-cadherin junctions as active mechanical integrators in tissue dynamics, Nat. Cell Biol. 17 (5) (2015) 533–539.
[28] L.L. Pontani, I. Jorjadze, J. Brujic, Cis and trans cooperativity of E-cadherin mediates adhesion in biomimetic lipid droplets, Biophys. J. 110 (2) (2016) 391–399.
[29] D.J. Cohen, M. Gloerich, W.J. Nelson, Epithelial self-healing is recapitulated by a 3D biomimetic E-cadherin junction, Proc. Natl. Acad. Sci. U. S. A. 113 (51) (2016) 14698–14703.
[30] D.P. Bi, J.H. Lopez, J.M. Schwarz, M.L. Manning, A density-independent rigidity transition in biological tissues, Nat. Phys. 11 (12) (2015) 1074 +.
[31] V. Maruthamuthu, B. Sabass, U.S. Schwarz, M.L. Gardel, Cell-ECM traction force modulates endogenous tension at cell-cell contacts, Proc. Natl. Acad. Sci. U. S. A. 108 (12) (2011) 4708–4713.
[32] V. Maruthamuthu, M.L. Gardel, Protrusive activity guides changes in cell-cell tension during epithelial cell scattering, Biophys. J. 107 (3) (2014) 555–563.
[33] S. Huveneers, J. de Rooij, Mechanosensitive systems at the cadherin-F-actin interface, J. Cell Sci. 126 (Pt 2) (2013) 403–413.
[34] D. Vestweber, R. Kemler, Identification of a putative cell adhesion domain of uvomorulin, EMBO J. 4 (13A) (1985) 3393–3398.